The 2021 Iteration of the TAMU Aerosol Refractive Index Database

Patrick Stegmann[a,*], Cheng Dang[b], and Benjamin Johnson[a]

[a]*NOAA Center for Weather and Climate Prediction, 5830 University Research Ct, College Park, MD 20740, USA*

[b]*University Corporation for Atmospheric Research,3090 Center Green Drive, Boulder, CO 80301, USA*

[*]*Presenting author (stegmann@ucar.edu)*

Theory:

The high variability of mineral dust composition makes obtaining information about its refractive index spectrum a particular challenge. Work by Stegmann and Yang (2017) suggests that there is no aerosol refractive index as such. Instead, the refractive index of an aerosol particle depends on its size and region of origin. A large dataset of composite minerals has been collected and combined using an Invariant Imbedding approach towards solving the Bruggeman equation:

$$\frac{d\varepsilon_{eff}(s)}{ds} = \frac{1}{3}\cdot\frac{\sum_{j=2}^{N} f_j \dfrac{\varepsilon_j - \varepsilon_{eff}(s)}{\varepsilon_j + 2\varepsilon_{eff}(s)}}{\sum_{j=1}^{N} f_j(s) \dfrac{\varepsilon_j}{\left[\varepsilon_j + 2\varepsilon_{eff}(s)\right]^2}}$$

This approach allows to compute an effective refractive index over a broad spectral range, upon which then the Kramers-Kronig relation is enforced. This approach is rigorous and enables sensitivity studies.

$$n(\nu) = 1 + \frac{2}{\pi} P \int_0^{\infty} \frac{\kappa^2 \cdot k(\kappa) - \nu \cdot \kappa \cdot k(\nu)}{\kappa^2 - \nu^2} d\ln\kappa$$

Data:

The model itself uses literature data for aerosol component chemical species from a variety of sources as a basis (see Fig. 1 & 2). These component species are then combined on the basis of an arbitrary, prescribed composition profile of the aerosol particle that may vary with particle size (see Fig. 3).

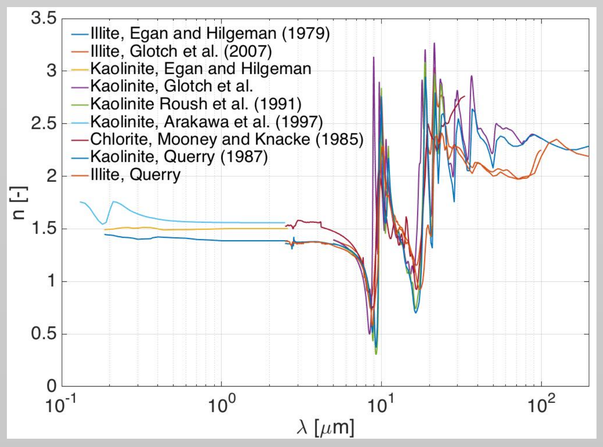

Fig. 1. Real part n(λ) of the refractive index spectrum of the Silicate group over the wavelength. Note the considerable difference between results from different studies.

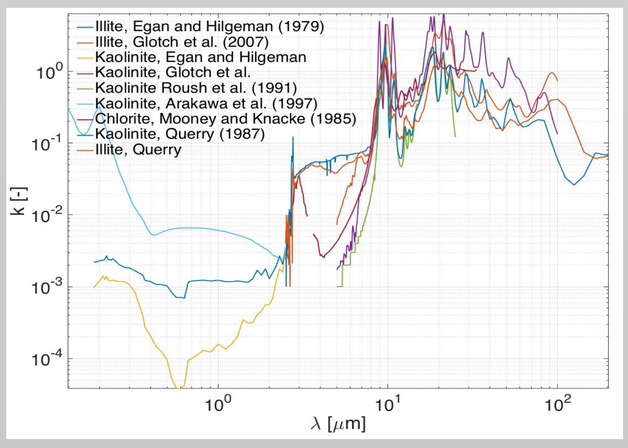

Fig. 2. Imaginary part k(λ) of the refractive index spectrum of the Silicate group over the wavelength. Considerable differences are again noticed in comparing the results obtained by different studies.

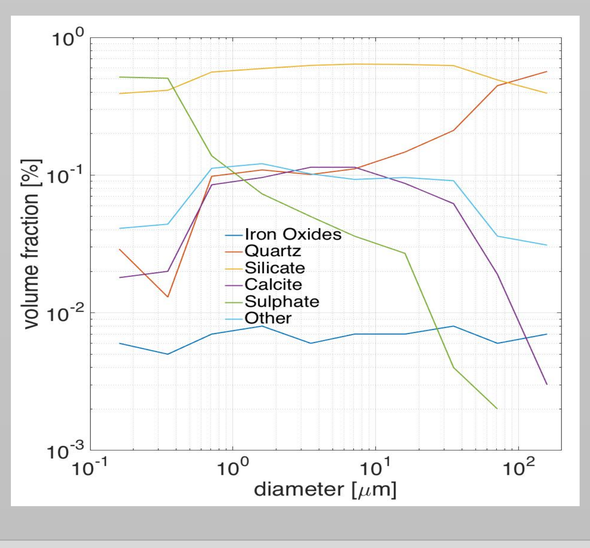

Fig. 3. Relative volume abundance over the geometrical diameter of a desert mineral dust particle from Kandler et al. (2009).

After the Bruggeman ODE is solved for a particular size/frequency combination, the resulting real part of the refractive index is computed using the Kramer—Kronig relationshio to ensure a physical spectrum. The outcome can then be compared with the original real part from the Bruggeman solution and eventual differences identified.

Computational Improvements:

As the model is parallel in both frequency space and the particle size dimension, the performance of the C++ code benefits greatly from OpenMP parallelization. Amdahl's law dictates the limitation of the code acceleration as a function of the parallelizable percentage of the code. The primary limitation here are the extensive data I/O processes. A further limitation on the hardware side is the number of available cores.

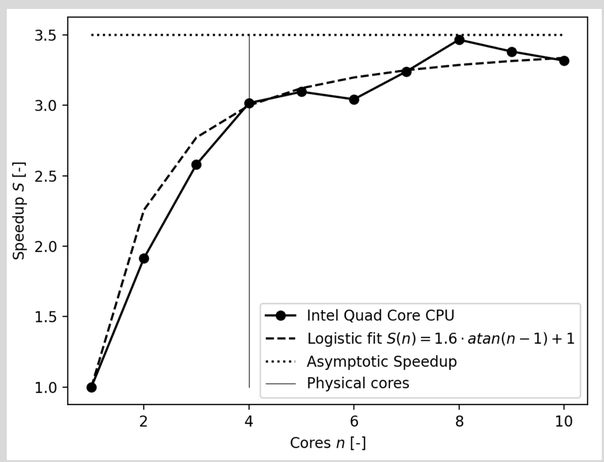

References:

[1] Stegmann, P., and P. Yang (2017): *A regional, size-dependant, and causal effective medium model for Asian and Saharan mineral dust refractive index spectra*. J. Aer. Sci. 114, 327-341.

Refractive Index Spectra:

For a. given particle composition it is possible to compute complex refractive index spectra between 0.1 and over 100 µm, depending on the chemical components. The impact of the variation of the aerosol particle size is illustrated in Fig. 4.

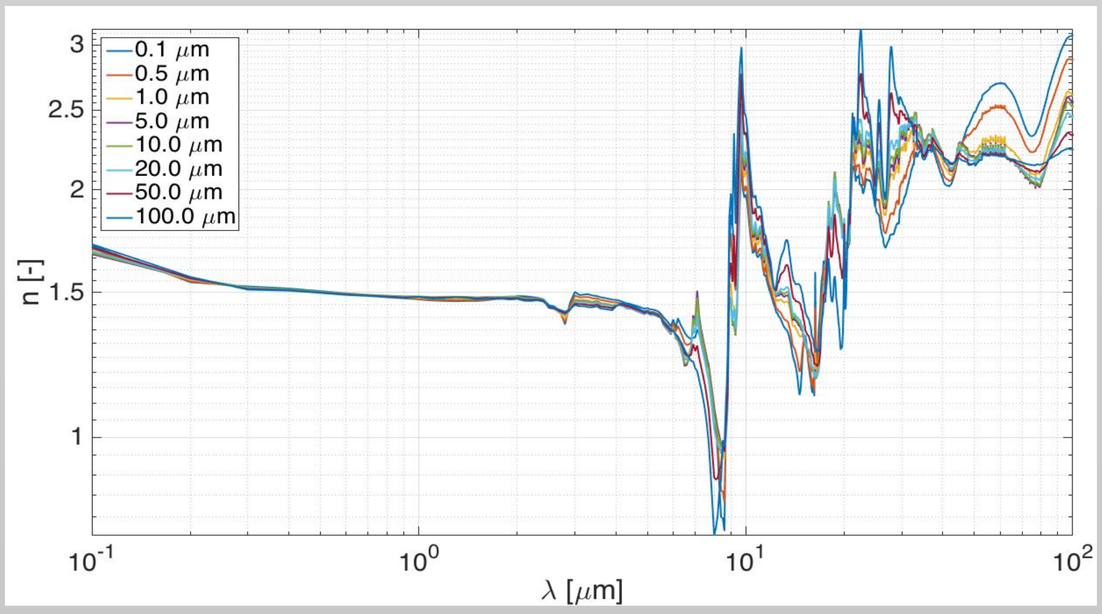

Fig. 4. Comparison of the real part of the refractive index spectrum of a northern Sahara dust aerosol particle for various particle sizes and thus mineral compositions computed using the Bruggeman EMA.

Choosing a aerosol particle size distribution such as the one in Fig. 5 also makes it possible to compute *size-effective* refractive index spectra, as illustrated in Fig. 6.

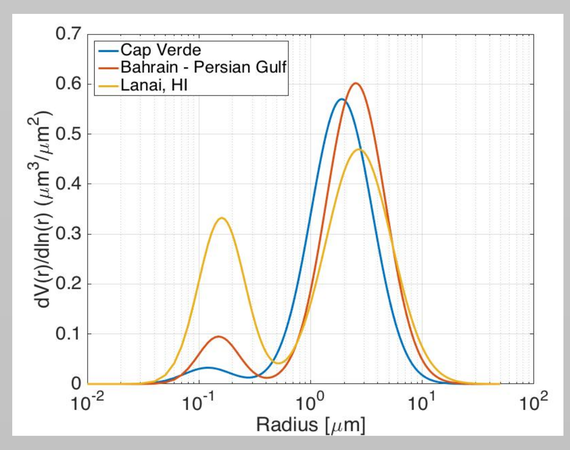

Fig. 5. Selection of bimodal size distributions from Dubovik et al. (2002) over the particle radius. On display are the distribution retrieved from AERONET measurements at Cap Verde, Bahrain, and Lanai.

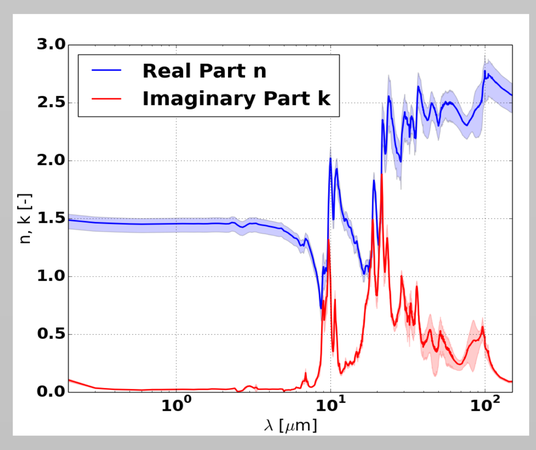

Fig. 6. Mean and three standard deviations of North Saharan mineral dust refractive index spectra

Uncertainty Analysis:

The formulation of the aerosol refractive index model allows to study the impact of uncertainties in the mineral component refractive index and volume fraction in a rigorous way, using Monte-Carlo analysis and a Tangent-Linear (TL) formulation.

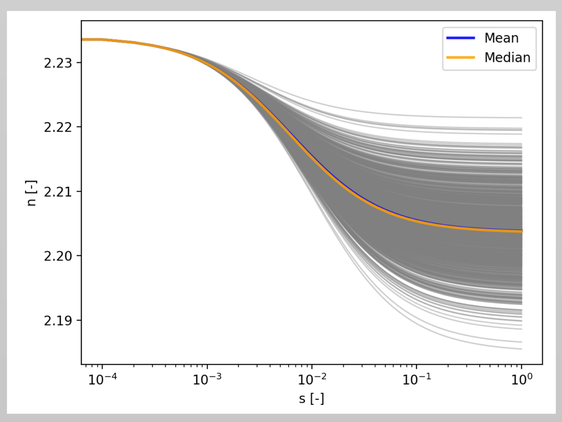

Fig. 7. Monte Carlo sensitivity analysis integration

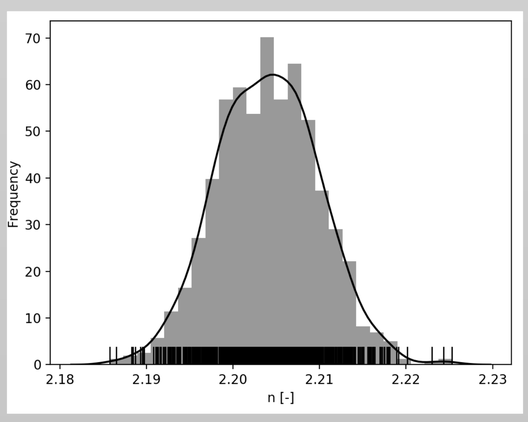

Fig. 8. Final Monte Carlo outcome distribution

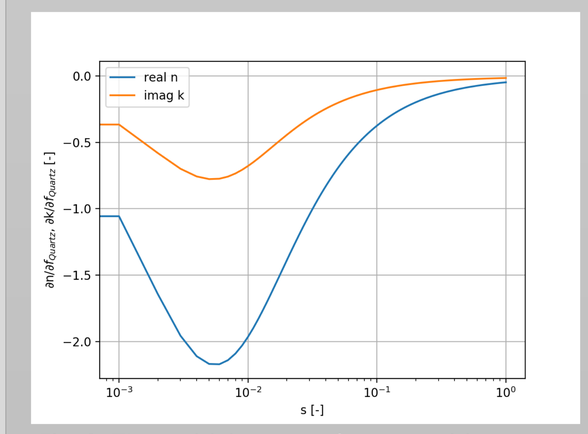

Fig. 9. TL sensitivity towards composition

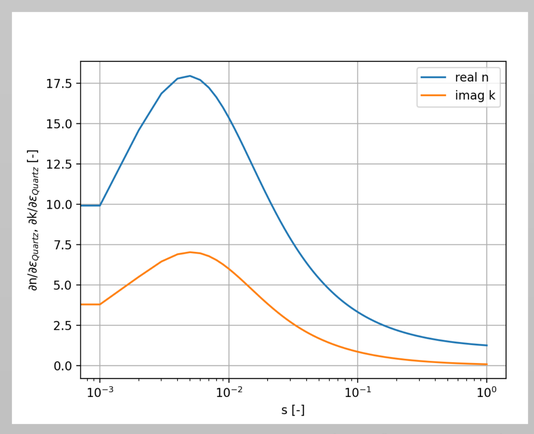

Fig. 10. TL sensitivity towards refractive index

Github Repository:

The code used in this poster is published as a Github repository. If you plan to use or modify the code or parts of it, please follow the online documentation:
https://github.com/PStegmann/Bruggeman_Effective_Medium